ELSEVIER

Chemical Geology 203 (2004) 305–317

CHEMICAL GEOLOGY
INCLUDING
ISOTOPE GEOSCIENCE

www.elsevier.com/locate/chemgeo

Helium and argon isotope geochemistry of alkaline intrusion-associated gold and copper deposits along the Red River–Jinshajiang fault belt, SW China

Rui-Zhong Hu[a,*], P.G. Burnard[b], Xian-Wu Bi[a], Mei-Fu Zhou[c], Jian-Tang Pen[a], Wen-Chao Su[a], Kai-Xing Wu[a]

[a] *Institute of Geochemistry, Chinese Academy of Sciences, 46 Road Guanshui-Guizhou Prov., Guiyang 550002, China*
[b] *Centre de Recherches Pétrographiques et Géochimiques (CRPG-CNRS), 15 rue Notre Dame des Pauvres, B.P. 20, 54501 Vandoeuvre-les-Nancy Cedex, France*
[c] *Department of Earth Sciences, The University of Hong Kong, Hong Kong, China*

Received 4 June 2003; accepted 17 October 2003

Abstract

The Red River–Jinshajiang strike-slip fault zone on the eastern margin of the Tibetan plateau was originally produced by the India–Eurasia collision ~ 60–70 Myr ago. Numerous post-collisional, mantle-derived alkaline igneous rocks, with ages of ~ 40–30 Ma, have been intruded along this fault zone. In recent years, several copper and gold deposits associated with the alkaline intrusions of this region were discovered, such as the Yao'an and Beiya gold deposits and the Yulong and Machangqing copper deposits studied in this paper. The mineralised intrusions are felsic, with SiO_2 ranging from 61.4 to 67.7 wt.%, K_2O+Na_2O from 8.1 to 11.5 wt.% and $K_2O/Na_2O>1$. The deposits are located at both the exo- and endo-contact zones of the intrusions. The mineral deposits are of hydrothermal origin, with the ore-forming temperatures mainly in the range 150–450 °C.

This paper presents He and Ar isotope analyses of these four deposits. The concentrations of ^4He trapped in fluid inclusions of pyrites from the ores are $(0.7–54.1)\times10^{-6}$ cm^3 STP g^{-1}, and those of ^{40}Ar are $(0.6–7.3)\times10^{-6}$ cm^3 STP g^{-1}, $^3He/^4He$ ratios are 0.3–2.5 Ra (Ra represents the $^3He/^4He$ ratio of air, 1.39×10^{-6}), $^{40}Ar/^{36}Ar$ ratios are 316–1736, and $^3He/^{36}Ar$ ratios are $0.2–11.2\times10^{-3}$. Generally, the $^3He/^4He$, $^{40}Ar/^{36}Ar$ and $^3He/^{36}Ar$ ratios for the gold deposits are higher than those for the copper deposits. We suggest that the ore-forming fluids of both gold and copper deposits were differentiated from the mantle-derived alkaline magmas, but were diluted by modified air-saturated water (MASW) that experienced intensive interaction with crustal rocks. However, the magmatic fluids responsible for the gold deposits were less extensively diluted by MASW, resulting in higher $^3He/^4He$, $^{40}Ar/^{36}Ar$ and $^3He/^{36}Ar$ ratios than the copper deposits.

Keywords: Red River–Jinshajiang; Alkaline intrusion; Copper and gold deposits; Helium and argon isotopes; Ore-forming fluid; Mantle fluids; ASW

* Corresponding author. Tel.: +86-851-5891962; fax: +86-851-5895574.
E-mail address: huruizhong@hotmail.com (R.-Z. Hu).

0009-2541/$ - see front matter © 2003 Elsevier B.V. All rights reserved.
doi:10.1016/j.chemgeo.2003.10.006

1. Introduction

Alkaline igneous rocks, such as shoshonites and alkaline porphyries, have recently attracted much attention among geoscientists worldwide, mainly due to their associated mineralization, and their importance in reconstructing the tectonic setting of ancient terranes into which they were intruded (Müller and Groves, 2000; Müller, 2002). It has been established in the past decade that these rocks are closely related to certain types of gold and base metal deposits (Sillitoe, 1997; Müller and Groves, 2000; Müller, 2002). In particular, some of the world's largest volcanic- and intrusive-hosted gold and copper deposits are intimately associated with alkaline igneous rocks (for details, see Müller, 2002). About 20% of the large gold deposits in the circum-Pacific region are associated with shoshonitic and alkaline rocks, which are unlikely to exceed 3% by volume of igneous rocks in subduction zones (Sillitoe, 1997). The increasing economic importance triggered research into the association between mineralization and alkaline magmatism (e.g. Lottermoser, 1990; Richards et al., 1991; Richards, 1992, 1993; Müller and Groves, 1993, 2000; Sillitoe, 1997, 2002; Jensen and Barton, 2000; Kelley and Ludington, 2002; Maughan et al., 2002; Müller et al., 2002; Strashimirov et al., 2002). In spite of the recent progress, there are several problems that remain to be resolved. For example, both gold and copper deposits are associated with alkaline intrusions, whereas the differences between gold- and copper-bearing fluids are still not well documented.

With the increasing knowledge in assessing modifications to noble gas isotopes by post-entrapment processes, noble gas isotopes have been employed to trace the origin of ore-forming fluids trapped as fluid inclusions in minerals since 1990s (Simmons et al., 1987; Turner and Bannon, 1991; Turner and Stuart, 1992; Turner et al., 1993; Stuart et al., 1994, 1995; Jean-Baptiste and Fouquet, 1996; Hu et al., 1998, 2003; Burnard et al., 1999; Kendrick et al., 2001). It is well known that there are large compositional differences between crustal- and mantle-derived He and Ar. In particular, a factor of $\sim$1000 times difference between $^{3}He/^{4}He$ ratios of upper mantle (6–9 Ra, where Ra is the atmospheric $^{3}He/^{4}He$ ratio, 1.39×10^{-6}: Stuart et al., 1995) and He produced in the crust (<0.05 Ra: Stuart et al., 1995) allows He to provide an unique insight into processes where mantle volatiles have been added to crustal fluids (Stuart et al., 1995). It has been suggested that alkaline rocks formed in four principal tectonic settings; continental arcs, post-collisional arcs, oceanic arcs and within-plate, and were all mantle-derived (Müller and Groves, 2000). Thus, if gold and copper deposits related to alkaline intrusions do have genetic links with mantle derived alkaline magmatism, their ore-forming fluids should reflect mantle-like He and Ar isotopes.

In recent years, several copper and gold deposits associated with alkaline intrusions were discovered in the Red River–Jinshajiang fault zone of SW China, which mainly consist of the Yao'an and Beiya gold deposits, and the Yulong and Machangqing copper deposits (Liang, 1992; Hu et al., 1998; Bi et al., 2002, in press(a); Hou et al., 2003). These deposits, located within or around the Tibetan plateau, have been poorly studied, and therefore the relationship between mineralization and alkaline magmatism has not been well recognised. In this paper, we present He and Ar isotope analyses for these four deposits, and use the noble gas data to constrain the origin of ore-forming fluids and to evaluate the possible differences between copper and gold ore fluids.

2. Geological background

The eastern part of the Tibetan plateau comprises several terranes, from north to south, Songpan-Ganzi, Qiangtang, Lhasa and Yangtze terranes (Fig. 1) which have been amalgamated together before Cretaceous time forming part of the Eurasian plate. At $\sim$60–70 Ma, the India–Eurasian collision created the plateau and resulted in eastward extrusion tectonics as well as forming the NW–WNW trending Red River–Jinshajiang fault zone (Fig. 1; Zhang et al., 1987; Turner et al., 1996; Chung et al., 1997, 1998; Yin and Harrison, 2000; Hou et al., 2003; Bi et al., in press(a)). Numerous alkaline igneous rocks occur along or near the fault zone (Fig. 1), forming a magmatic belt extending over 1000 km in length and generally about 50–80 km wide. K–Ar and Ar–Ar dating of whole rock or mineral samples from the alkaline rocks define intrusion ages of $\sim$40–30 Ma (Zhang and Xie, 1997; Chung et al., 1998; Wang et al., 2001).

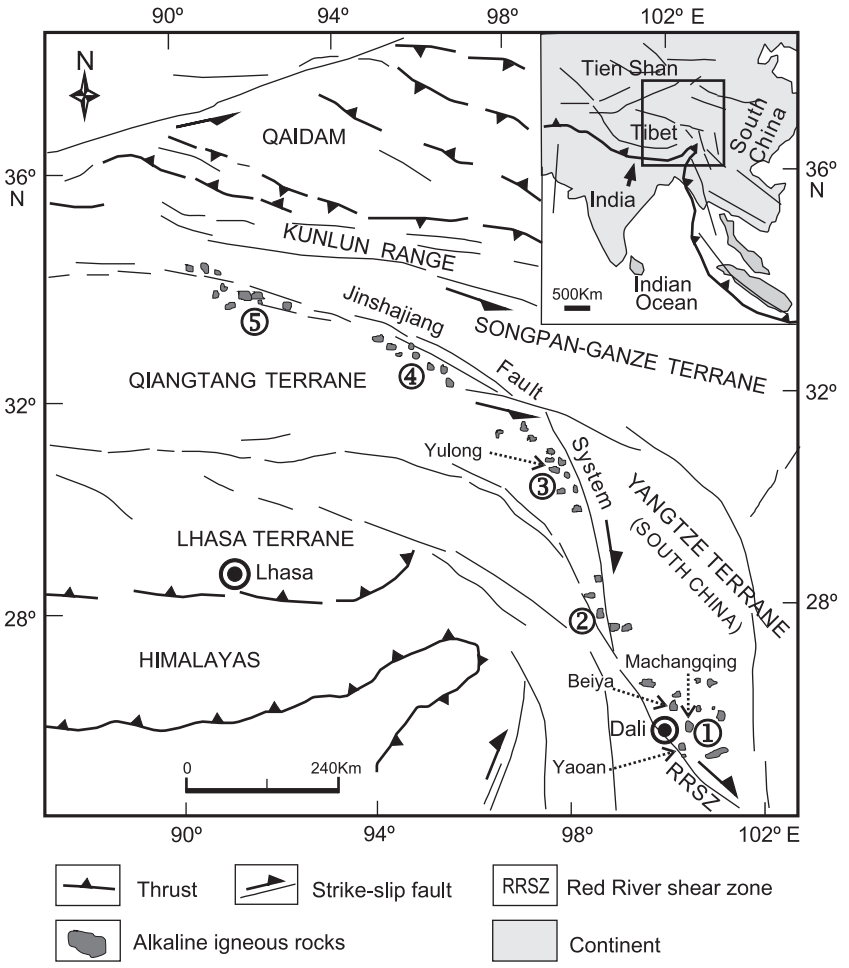

Fig. 1. A sketch geological map of the Red River–Jinshajiang fault zone showing the locations of alkaline igneous rocks and related ore deposits (modified from Chung et al., 1998).

The alkaline rocks, divided into five groups (1–5 in Fig. 1), are exposed around two tectonic belts, the Red River shear zone and the Jinshajiang fault system (Fig. 1). Geochemically, these volcanic and intrusive rocks range from basaltic to trachytic and rhyolitic composition (Zhang et al., 1987; Chung et al., 1998). They show ultra-potassic or shoshonitic character and incompatible trace element variation patterns, with highly enriched large-ion lithophile elements, light rare earth elements, and depleted high field strength elements (Chung et al., 1998; Hou et al., 2003; Bi et al., in press(b). Isotopically, their Sr–Nd compositions lie close to the range for type II enriched mantle (Zhang and Xie, 1997; Zhang et al., 1998; Hou et al., 2003), characterized by highly radiogenic Sr ($^{87}Sr/^{86}Sr \leq 0.708$) with intermediate Nd isotopic composition. The above features support the origin of these alkaline magmas from a metasomatized lithospheric-mantle which was previously contaminated by subducted oceanic slab (Zhang et al., 1987; Chung et al., 1998; Hou et al., 2003; Bi et al., in press(b)). A series of Tertiary rift basins, the eruption of alkaline basalts and the positive gravity anomaly along the Red River–Jinshajiang fault system suggest that the alkaline rocks formed in a post-collisional extensional setting (Tu et al., 1984; Zhang et al., 1987; Turner et al., 1996; Chung et al., 1997, 1998; Deng et al., 1998, Hou et al., 2003; Bi et al., in press(b)).

Within the group 1, the Beiya and Yao'an gold deposits and Machangqing copper deposit are associated with the Beiya, Yao'an and Machangqing alkaline intrusions, respectively. The Yulong copper deposit is hosted in the Yulong alkaline intrusion of group 3 (Fig. 1). As parts of the Red River–Jinahajiang alkaline igneous belt, these gold and copper-mineralized alkaline intrusions share similar geochemical and tectonic characteristics with the remainder of the belt. The mineralized intrusions are all felsic, with SiO_2 ranging from 61.4 to 67.7 wt.%, $K_2O + Na_2O$ from 8.1 to 11.5 wt.% and $K_2O/Na_2O>1$ (Table 1). Lithologically, the mineralized rocks are mostly composed of syenite porphyry and quartz syenite porphyry in the Yao'an and Beiya gold deposits, and monzogranite porphyry and alkaline granoporphyry in the Yulong and Machangqing copper deposits (Table 1). In addition, as reflected by Table 1, (1) both gold and copper deposits studied in this work essentially belong to the porphyry type (Hou et al., 2003; Bi et al., in press(a)); (2) the alteration pattern is similar to those developed in porphyry deposits related to calc-alkaline rocks, except of the poor development of silicification in gold deposits; (3) the deposits are all located at both the exo- and endo-contact zones of alkali-porphyry intrusions, and are controlled by fractures and faults; and (4) they are all hydrothermal in origin, with ore-forming temperatures ~ 150–450 °C.

3. Analytical methods

Approximately 200 mg of separated coarse (>1 mm, but the coarser the better) pyrite grains were cleaned ultrasonically in alcohol, dried, then loaded in on-line in vacuo crushers similar to those described in Burnard et al. (1993). The samples were baked at 120 °C for 6–8 h prior to analysis in order to remove adhered atmospheric contaminants. Gases were released from the grains into the all metal extraction system by sequentially crushing in modified Nupro type valves; the released gases were purifed with two

Table 1
Geological features of the alkaline intrusion-related ore deposits along the Red River–Jinshajiang belt, SW China

Deposits	Copper deposits		Gold deposits	
	Yulong	Machangqing	Yao'an	Beiya
Wall rocks	Triassic limestones	Ordovician clastics; Devonian limestones	Jurassic mudstones	Triassic limestones
Alkaline intrusions (individual outcrop area)	Monzogranite porphyry; Qtz monzogranite porphyry (< 1 km^2); SiO_2: 67.1 %, $K_2O + Na_2O$: 8.3%	Granite porphyry; syenite porphyry (< 1 km^2); SiO_2: 67.7%, $K_2O + Na_2O$: 8.1%	Qtz syenite porphyry; syenite porphyry (< 1 km^2); SiO_2: 61.4%, $K_2O + Na_2O$: 9.6%	Syenite porphyry (< 0.5 km^2); SiO_2: 66.5%, $K_2O + Na_2O$: 11.5%
Mineralized location	Exo- and endo-contact zone	Exo- and endo-contact zone	Exo- and endo-contact zone	Exo- and endo-contact zone
Ore-controlling structure	Fractures, faults	Fractures, faults	Fractures, faults	Fractures, faults
Alteration zoning (Outward from center)	K silicate → qtz-ser → argillic-propylitic	K silicate → qtz-ser → argillic-propylitic	K silicate → argillic-propylitic	K silicate → argillic-propylitic
Orebody shape	Stratiform in skarn; lenticular in porphyry	Lenticular and vein	Lenticular and vein	Lenticular and vein
Ore structure	Disseminated, veinlet	Disseminated, veinlet	Veinlet, disseminated	Veinlet, disseminated
Mineral assemblage*	chal + mo + py + born + mag + qtz + cal	chal + mo + py + born + mag + qtz + cal	py + he + ga + chal ± qtz ± cal	py + he + ga + chal ± qtz ± cal
Tonnage, grade	6.22 Mt Cu, Cu: 1.0%	0.25 Mt Cu, Cu: 0.8%	10 t Au, Au: 4–5 ppm	60 t Au, Au: 5–6 ppm
Element association	Cu + Mo ± Au	Cu + Mo ± Au	Au ± Ag + Pb ± Cu	Au ± Ag + Pb ± Cu
Temperature	160–600 °C	250–430 °C	150–310 °C	120–420 °C

chal = chalcopyrite, mo = molybdenite, py = pyrite, born = bornite, mag = magnetite, he = hematite, ga = galena, qtz = quartz, cal = calcite, ser = sericite, Mt = million ton. Data are mainly from Rui and Huang (1984), Zhang et al. (1987), Liang (1992), Ye et al. (1992), Tang and Lo (1995), Hu et al. (1998), Bi et al. (2002, in press(a,b), and Hou et al. (2003).

SAES Zr–Al getters (one at room temperature, the other at 450 °C). Argon was adsorbed on charcoal at 77 K prior to analysis on a modified 12 cm, 90° nuclide mass spectrometer. Helium was separated from Ne with a separate charcoal trap at 35 K prior to analysis on a MAP-215 mass spectrometer. Blanks were estimated for every sample analysed by executing the exact same procedure as the crush step, with the exception of compressing the sample. Helium blanks were negligible (^{3}He blank $<3\times10^{-16}$ cm^3 STP); samples were corrected for Ar blank contributions which were typically $<0.4\times10^{-9}$ cm^3 ^{40}Ar STP (<2% of any crushing step). The system was calibrated using a reservoir of reduced pressure air to which He (^{3}He/^{4}He = 2.04 Ra) had been added to produce a ^{4}He/^{40}Ar ratio of 1.42; all other isotopic and abundance ratios were atmospheric. Aliquots of 0.1 cc ^{40}Ar were delivered by the micropipetting system, but calibrations were also performed on subsplits of this in order to correct for pressure-dependent discrimination effects in the MAP source (Burnard and Farley, 2000).

4. Results and discussion

4.1. The "initial" He and Ar compositions of the ore-forming fluids

The results of He and Ar isotope analyses of fluid inclusions in pyrite from the deposits are listed in Table 2. The concentrations of ^{4}He are $(0.7–54.1)\times10^{-6}$ cm^3 STP g^{-1} and those of ^{40}Ar are $(0.6–7.3)\times10^{-6}$ cm^3 STP g^{-1}. The large variations in noble gas concentrations probably reflect variations in fluid inclusion density and are unlikely to have genetic implications. Noble gas isotopic ratios are more consistent: ^{3}He/^{4}He ratios are 0.3–2.5 Ra (Ra represents the ^{3}He/^{4}He ratio of air, 1.39×10^{-6}), ^{40}Ar/^{36}Ar ratios are 316–1736, and ^{3}He/^{36}Ar ratios are $0.2–11.2\times10^{-3}$. Generally, the ^{3}He/^{4}He, ^{40}Ar/^{36}Ar and ^{3}He/^{36}Ar ratios of the gold-related fluids are higher than those of the copper-related fluids.

The measured ^{3}He/^{4}He values of different crushing steps (i.e., crushing 1, crushing 2, etc.) for each sample are typically within error, and there is no significant decrease in ^{3}He/^{4}He with increasing degree of crushing (Table 2); therefore, in situ ^{4}He produced by decay of U and Th within the mineral lattice after formation is negligible, and the He released by crushing is dominantly from fluid inclusions (Stuart et al., 1995; Hu et al., 1998, 2003; Burnard et al., 1999). The deposits studied are relatively young (less than 40 Ma), and the U concentration in inclusion trapped fluid is relatively low (less than 3 ppm); therefore, in situ produced ^{4}He within fluid inclusions themselves is also negligible (Simmons et al., 1987; Hu et al., 1998; Burnard et al., 1999). Pyrite is known to be a suitable noble gas trap (Stuart et al., 1994; Jean-Baptiste and Fouquet, 1996; Hu et al., 1998, 2003; Burnard et al., 1999), with inclusion trapped He (and Ar) unlikely to be extensively lost within ~ 100 Ma (Burnard et al., 1999; Hu et al., 2003). In addition, the pyrite samples analyzed were all collected from underground workings; therefore, cosmogenic ^{3}He can be ruled out (Simmons et al., 1987; Stuart et al., 1995). Therefore, it is likely that the measured He abundances and isotopic compositions of the samples listed in Table 2 represent the initial values of primary fluid inclusions or ore-forming fluids of the deposits.

Contributions of in situ produced ^{40}Ar from the mineral lattice to the measured ^{40}Ar/^{36}Ar ratios is thought unlikely due to the low diffusivity of Ar in pyrite (York et al., 1982; Smith et al., 2001) and the low K content of pyrite. Although in-situ radiogenic ^{40}Ar growth in fluid inclusions from dissolved K or K-bearing minerals cannot be ruled out, the amount of in-situ radiogenic ^{40}Ar in fluid inclusions trapped in K-free minerals (such is the case in the present study) should be negligible (Turner and Wang, 1992; Qiu, 1996).

On the other hand, measured ^{40}Ar/^{36}Ar ratios will be lower than the true ^{40}Ar/^{36}Ar ratio of the fluid due to contributions of atmospheric Ar (Burnard et al., 1999). In addition to the ^{40}Ar/^{36}Ar ratios of the mineralizing fluids, the measured ^{40}Ar/^{36}Ar ratio is also affected by atmospheric ^{36}Ar either present as a surface adsorbed component or trapped in secondary fluid inclusions of atmospheric origin. As secondary fluid inclusions are usually distributed linearly along micro-fissures in the minerals, the finer the minerals are crushed (or the more times the minerals are crushed), the lower the contribution from secondary, low ^{40}Ar/^{36}Ar fluid inclusions (Hu et al., 2003). Therefore, atmospheric ^{36}Ar in secondary fluid inclusions would be expected to be released earlier in the

Table 2
He and Ar isotopic compositions of inclusion-trapped fluid in pyrites[a]

Deposits	Sample	Crushing number	Weight[b] (g)	^{4}He[c] (cm^3 STP)	^{40}Ar[c] (cm^3 STP)	$^{40}Ar/^{36}Ar$	$^3He/^4He$ (Ra)	$^{40}Ar^*/^4He$[d]	$^3He/^{36}Ar$ (10^{-3})	^{4}He (cm^3 STPg^{-1})	^{40}Ar (cm^3 STPg^{-1})
Yao'an Au	YA43	1		1.25E − 07	1.58E − 07	464.3 ± 18.2	2.03 ± 0.15	0.46 ± 0.03	1.04 ± 0.07		
		2		1.04E − 07	1.69E − 07	408.9 ± 18.1	2.30 ± 0.17	0.45 ± 0.04	0.81 ± 0.05		
		3		4.88E − 08	6.07E − 08	527.8 ± 19.0	1.84 ± 0.14	0.55 ± 0.04	1.09 ± 0.07		
		Total[e]	0.0879	2.78E − 07	3.87E − 07	446.4 ± 11.8	2.10 ± 0.10	0.47 ± 0.02	0.94 ± 0.04	3.16E − 06	4.01E − 06
	LJ49-3	1		9.85E − 08	1.3E − 07	353.5 ± 15.7	0.31 ± 0.03	0.22 ± 0.03	0.12 ± 0.01		
		2		1.69E − 07	1.6E − 07	387.2 ± 15.9	0.33 ± 0.03	0.22 ± 0.02	0.19 ± 0.01		
		Total	0.0658	2.67E − 07	2.89E − 07	371.3 ± 11.2	0.32 ± 0.02	0.22 ± 0.02	0.15 ± 0.01	4.06E − 06	4.39E − 06
	YA36-1	1		3.19E − 07	2.3E − 07	565.2 ± 21.7	2.39 ± 0.17	0.35 ± 0.02	2.60 ± 0.16		
		2		4.04E − 07	2.66E − 07	605.5 ± 24.8	2.44 ± 0.18	0.34 ± 0.02	3.12 ± 0.20		
		Total	0.0828	7.22E − 07	4.97E − 07	586.1 ± 16.5	2.42 ± 0.12	0.34 ± 0.02	2.87 ± 0.13	8.72E − 06	6.00E − 06
	YA36	1		2.14E − 08	1.63E − 08	330.8 ± 12.4	2.48 ± 0.22	0.08 ± 0.01	1.49 ± 0.12		
		2		2.16E − 07	1.95E − 07	425.8 ± 18.9	2.41 ± 0.18	0.28 ± 0.02	1.58 ± 0.10		
		3		4.58E − 08	1.25E − 08	385.9 ± 14.5	1.57 ± 0.13	0.06 ± 0.01	3.09 ± 0.22		
		4		4.87E − 08	1.14E − 08	589.6 ± 21.4	2.20 ± 0.17	0.12 ± 0.01	7.69 ± 0.53		
		Total	0.0321	3.32E − 07	2.35E − 07	420.7 ± 15.4	2.26 ± 0.12	0.21 ± 0.01	1.87 ± 0.09	1.03E − 05	7.32E − 06
	YA47C	1		2.46E − 07	1.67E − 07	605.0 ± 23.2	2.27 ± 0.16	0.35 ± 0.02	2.82 ± 0.17		
		2		8.84E − 08	4.29E − 08	625.8 ± 23.0	1.81 ± 0.14	0.26 ± 0.02	3.25 ± 0.21		
		Total	0.0926	3.35E − 07	2.09E − 07	609.2 ± 19.2	2.15 ± 0.12	0.32 ± 0.02	2.91 ± 0.15	3.61E − 06	2.26E − 06
	YA65-1	1		3.81E − 07	2.1E − 07	1069.4 ± 40.8	2.179 ± 0.16	0.40 ± 0.02	5.84 ± 0.36		
		2		2.06E − 07	8.56E − 08	1735.5 ± 65.9	1.93 ± 0.14	0.34 ± 0.02	11.21 ± 0.69		
		Total	0.1426	5.88E − 07	2.96E − 07	1202.9 ± 37.2	2.08 ± 0.11	0.38 ± 0.02	6.91 ± 0.33	4.12E − 06	2.07E − 06
	YA65	1		3.65E − 07	4.02E − 07	438.3 ± 52.2	2.48 ± 0.18	0.36 ± 0.03	1.37 ± 0.18		
		2		2.06E − 07	1.71E − 07	625.4 ± 27.7	2.50 ± 0.18	0.44 ± 0.03	2.62 ± 0.17		
		3		4.61E − 08	3.86E − 08	674.4 ± 24.4	2.21 ± 0.17	0.47 ± 0.03	2.47 ± 0.17		
		4		4.5E − 08	n[f]		2.11 ± 0.17				
		5		4.9E − 08	n		2.21 ± 0.17				
		Total	0.1402	7.11E − 07			2.43 ± 0.11			5.07E − 06	
	YA29-1	1		1.42E − 07	2.14E − 07	450.2 ± 21.0	2.44 ± 0.18	0.52 ± 0.04	1.01 ± 0.07		
		2		6.57E − 08	6.89E − 08	424.5 ± 16.6	2.31 ± 0.18	0.32 ± 0.03	1.30 ± 0.09		
		Total	0.0683	2.08E − 07	2.83E − 07	443.7 ± 16.1	2.40 ± 0.13	0.45 ± 0.03	1.09 ± 0.06	3.04E − 06	4.14E − 06
Beiya Au	WD28-3	1		6.01E − 07	3.53E − 07	520.1 ± 40.0	1.30 ± 0.09	0.25 ± 0.02	1.60 ± 0.15		
		2		4.22E − 08	4.75E − 08	884.8 ± 41.1	1.86 ± 0.15	0.75 ± 0.05	2.03 ± 0.15		
		3		6.8E − 08	4.9E − 08	1051.6 ± 44.6	1.94 ± 0.15	0.52 ± 0.03	3.93 ± 0.25		
		Total	0.0625	7.12E − 07	4.5E − 07	577.0 ± 38.6	1.40 ± 0.08	0.31 ± 0.02	1.77 ± 0.14	1.14E − 05	7.20E − 06

	WD11	1		4.27E − 07	6.78E − 07	383.5 ± 19.7	1.90 ± 0.14	0.36 ± 0.06	0.64 ± 0.04		
		2		1.27E − 07	9.16E − 8	563.4 ± 21.4	1.80 ± 0.13	0.34 ± 0.02	1.95 ± 0.12		
		3		5.25E − 08	6.46E − 08	551.4 ± 24.6	1.90 ± 0.16	0.57 ± 0.05	1.19 ± 0.09		
		Total	0.112	6.06E − 07	8.34E − 07	543.3 ± 23.2	1.88 ± 0.10	0.38 ± 0.04	0.77 ± 0.04	5.41E − 05	6.00E − 07
	WD17	3		5.48E − 07	1.11E − 06	348.0 ± 13.6	1.96 ± 0.14	0.31 ± 0.04	0.47 ± 0.03		
		2		2.17E − 07	1.18E − 07	845.9 ± 33.0	1.99 ± 0.15	0.35 ± 0.02	4.31 ± 0.27		
		Total	0.1679	7.66E − 07	1.23E − 06	368.8 ± 13.6	1.97 ± 0.11	0.32 ± 0.03	0.63 ± 0.03	4.56E − 06	7.33E − 06
	WD28-5	1		2.77E − 07	3.54E − 07	391.6 ± 76.7	1.62 ± 0.12	0.31 ± 0.03	0.69 ± 0.14		
		2		1.41E − 07	1.27E − 07	431.6 ± 19.3	1.56 ± 0.12	0.28 ± 0.02	1.04 ± 0.07		
		Total	0.1696	4.18E − 07	4.82E − 07	401.4 ± 59.4	1.60 ± 0.08	0.30 ± 0.02	0.77 ± 0.12	2.46E − 06	2.84E − 06
Yulong Cu	PD8-1	1		5.26E − 08	5.3E − 08	422.7 ± 17.8	0.65 ± 0.06	0.30 ± 0.03	0.38 ± 0.03		
		2		9.1E − 08	3.84E − 08	388.2 ± 15.3	0.42 ± 0.04	0.10 ± 0.01	0.54 ± 0.05		
		3		6.66E − 08	2.87E − 08	361.6 ± 13.4	0.52 ± 0.05	0.08 ± 0.01	0.60 ± 0.05		
		Total	0.0922	1.58E − 07	6.71E − 08	376.4 ± 10.3	0.46 ± 0.03	0.09 ± 0.01	0.57 ± 0.04	1.71E − 06	7.28E − 07
	ZK59-16	1		5.08E − 08	4.73E − 08	455.6 ± 17.3	1.58 ± 0.13	0.32 ± 0.02	1.08 ± 0.08		
		2		3.51E − 08	n		1.03 ± 0.09				
		3		2.49E − 08	n		0.79 ± 0.09				
		Total	0.0966	1.11E − 07			1.23 ± 0.07			1.15E − 06	
	ZK59-11	1		5.2E − 08	1.52E − 07	315.6 ± 14.3	1.50 ± 0.12	0.18 ± 0.06	0.23 ± 0.02		
		2		2.27E − 08	4.01E − 08	414.8 ± 16.3	1.41 ± 0.13	0.51 ± 0.04	0.46 ± 0.04		
		Total	0.1134	7.46E − 08	1.92E − 07	332.2 ± 12.6	1.47 ± 0.09	0.28 ± 0.04	0.26 ± 0.02	6.58E − 07	1.69E − 06
	W81	1		2.4E − 07	1.08E − 07	630.1 ± 24.7	0.45 ± 0.04	0.24 ± 0.01	0.88 ± 0.06		
		2		8.27E − 08	4.15E − 08	643.0 ± 26.5	0.64 ± 0.06	0.27 ± 0.02	1.15 ± 0.09		
		Total	0.0571	3.23E − 07	1.5E − 07	633.6 ± 18.9	0.50 ± 0.03	0.25 ± 0.01	0.96 ± 0.05	5.66E − 06	2.62E − 06
	W4	1		1.86E − 07	1.97E − 07	377.8 ± 23.3	1.58 ± 0.12	0.23 ± 0.03	0.78 ± 0.06		
		2		1.07E − 07	9.98E − 08	376.2 ± 15.3	1.52 ± 0.12	0.20 ± 0.02	0.86 ± 0.06		
		3		3.71E − 08	3.32E − 08	404.7 ± 16.0	1.51 ± 0.14	0.24 ± 0.02	0.95 ± 0.08		
		4		3.21E − 08	1.61E − 08	515.7 ± 20.2	1.10 ± 0.09	0.21 ± 0.01	1.58 ± 0.12		
		5		7.26E − 08	4.05E − 08	370.7 ± 14.4	1.44 ± 0.11	0.11 ± 0.01	1.33 ± 0.09		
		Total	0.0804	4.36E − 07	3.87E − 07	383.0 ± 13.0	1.50 ± 0.06	0.20 ± 0.01	0.90 ± 0.04	5.42E − 06	4.81E − 06

[a] Analyzed at Caltech, USA.

[b] Sample weights are the fraction of crushed pyrite that passes through a 100 μ sieve.

[c] Uncertainties in noble gas concentrations are ≈ 5%; quoted errors in isotope ratios are 1σ.

[d] $^{40}Ar^{*}$ refers to the excess Ar.

[e] Totals are the sums of all crushes.

[f] Not analyzed.

crushing schedule. From Table 2, it can be seen that, with increasing degree of crushing, the $^{40}Ar/^{36}Ar$ ratios of the samples tend to increase, indicating that the Ar isotopic compositions of earlier crushings have been more influenced by atmospheric ^{36}Ar. Therefore, Ar released by the last crushing step will be most representative of the inclusion-trapped fluids; the remaining values are of no primary significance. Because of this reason, only He and Ar isotopic compositions of the last crushing step for each sample are adopted for further discussions, which are plotted in Figs. 2–5 (but for samples YA65 and ZK59-16, the crushing 3 and crushing 1 data were used due to the lack of Ar data of later crushes for these two samples).

4.2. The sources of He and Ar

Helium in the atmosphere is too low to exert a significant influence on He abundances and isotopic compositions of most crustal fluids (Marty et al., 1989; Stuart et al., 1994). As a result, He in these ore-forming fluids have only two possible sources: mantle-derived He and radiogenic He produced in the crust (Turner et al., 1993). The $^{3}He/^{4}He$ ratio produced in the crust depends on the Li concentration due to $^{6}Li(n,\alpha)^{3}H(\beta)^{3}He$ reactions, but generally these reactions are only significant in Li-rich minerals (Ballentine and Burnard, 2002). Due to the lack of Li minerals, $^{3}He/^{4}He$ ratios in the crust of these areas should be similar to the characteristic values of the crust, i.e., $^{3}He/^{4}He < 0.05$ Ra (Mamyrin and Tolstikhin, 1984; Turner et al., 1993). As can be seen from Table 2, $^{3}He/^{4}He$ ratios of the ore-forming fluids from the four studied deposits (0.3–2.5 Ra) are much higher than those of the crust, but lower than those of the subcontinental mantle ($^{3}He/^{4}He \approx 6$ Ra; Dunai and Baur, 1995; Gautheron and Moreira, 2002), demonstrating that these ore fluids contain mantle- and crustal-derived He. In addition, there is an obvious positive correlation between He and Ar isotopic compositions (Figs. 2–5), consistent with two component mixing between high $^{3}He/^{4}He$, high $^{40}Ar/^{36}Ar$ mantle-derived fluids and a crustal fluid with low $^{3}He/^{4}He$ and near atmospheric $^{40}Ar/^{36}Ar$ that is best described as "modified air saturated water".

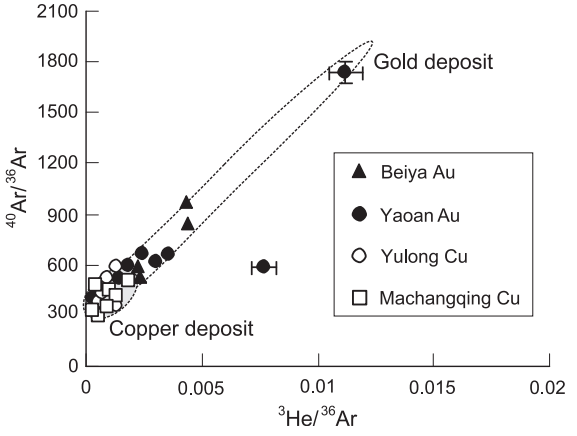

Fig. 2. $^{3}He/^{36}Ar$ vs. $^{40}Ar/^{36}Ar$ plot of inclusion fluids in pyrites. Data from the Machanging copper deposit are taken from Hu et al. (1998). Least square fit to the data has the equation: $^{40}Ar/^{36}Ar = (1.28 \times 10^{5})\ ^{3}He/^{36}Ar + 319.36$, $\gamma^{2} = 0.93$. The range in compositions result from mixing of a ^{3}He-, ^{40}Ar-rich "magmatic" fluid with a ^{36}Ar-dominated surface derived fluid. The $^{3}He/^{36}Ar$ ratio of surface derived fluids is low ($\approx 10^{-8}$); therefore, the $^{40}Ar/^{36}Ar$ ratio of the surface derived fluid will be that of the intercept (=320). Sample YA36 has been excluded from the regression as this clearly lies in a different population. Multiple crushes of YA36 (Table 2) resulted in extreme variations in $^{40}Ar^{*}/^{4}He$ ratios, suggesting there has been some He–Ar fractionation which could have altered the trapped $^{3}He/^{36}Ar$ ratio.

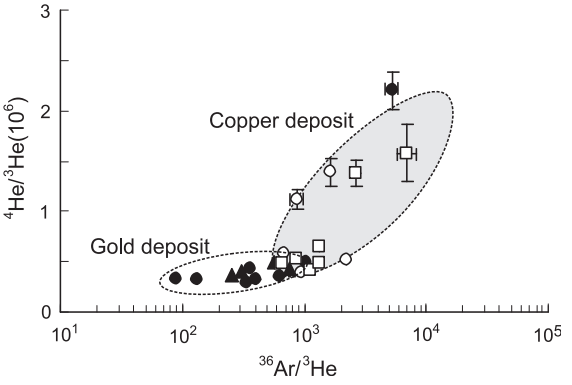

Fig. 3. $^{36}Ar/^{3}He$ vs. $^{4}He/^{3}He$ plot of inclusion trapped fluids in pyrite. Symbols and the Machangqing data source are the same as in Fig. 2. Least square fit to the data has the equation: $^{4}He/^{3}He = 255.26 \times (^{36}Ar/^{3}He) + 3.06 \times 10^{5}$ ($\gamma^{2} = 0.69$).

4.2.1. Component 1: modified air-saturated water (MASW)

Pure air-saturated water (PASW) (meteoric or marine) is characterized by atmospheric He and Ar isotope compositions ($^{3}He/^{4}He = 1.39 \times 10^{-6} = 1$ Ra, $^{40}Ar/^{36}Ar = 295.5$, $^{3}He/^{36}Ar \approx 5 \times 10^{-8}$) (Turner et

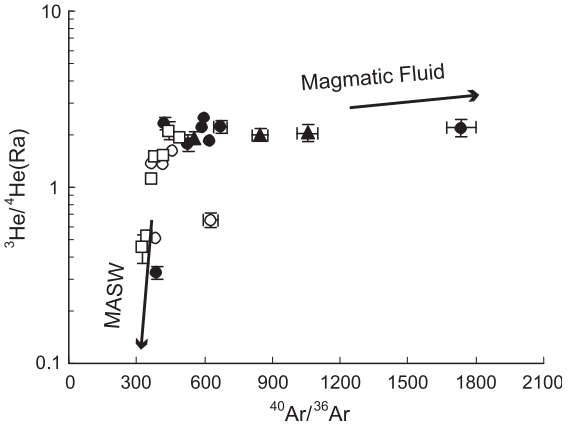

Fig. 4. ^{40}Ar/^{36}Ar vs. ^{3}He/^{4}He (Ra) plot of inclusion trapped fluids in pyrite. Symbols and the Machangqing data source are the same as in Fig. 2.

al., 1993; Stuart et al., 1995; Burnard et al., 1999). The crustal fluid trapped in these fluid inclusions is PASW that has clearly been modified by addition of radiogenic ^{4}He and (to a lesser extent) of radiogenic ^{40}Ar. However, the ^{3}He/^{36}Ar of the MASW fluid is unlikely to be changed (as both ^{3}He and ^{36}Ar are unradiogenic). Therefore, the trends in Figs. 2 and 3 can be extrapolated to the ^{3}He/^{36}Ar value of PASW (5×10^{-8}), in order to calculate the MASW ^{3}He/^{4}He < 0.05 Ra and ^{40}Ar/^{36}Ar $\approx$ 320. The ^{3}He/^{4}He ratio of this fluid is typical of crustally produced He, suggesting that the fluid interacted with crustal rocks and obtained "excess" radiogenic ^{4}He from the crust. In contrast, the ^{40}Ar/^{36}Ar value of MASW is close to the Ar isotopic composition of PASW (^{40}Ar/^{36}Ar $\approx$ 295.5) but contains resolvable radiogenic ^{40}Ar (^{40}Ar*; ^{40}Ar* is calculated assuming that all ^{36}Ar is atmospheric in origin, i.e. ^{40}Ar* = ^{40}Ar − [^{36}Ar·295.5]). The trend in Fig. 5 can also be extended to this modified air-saturated fluid. A ^{4}He/^{40}Ar* ratio of 0.01–0.05 is obtained from the (albeit poor) correlation between ^{3}He/^{4}He and ^{40}Ar*/^{4}He (Fig. 5), similar to but a little bit lower than estimates of the likely instantaneous ^{40}Ar*/^{4}He production ratio of the crust ($\approx$ 0.2; Torgersen et al., 1988; Ballentine and Burnard, 2002). Previous studies have demonstrated that contemporary groundwaters commonly have low ^{40}Ar*/^{4}He due to preferentially acquiring ^{4}He relative to ^{40}Ar from crustal rocks, because of the higher closure temperature of Ar relative to He (Torgersen et al., 1988; Ballentine and Burnard, 2002). For the majority of minerals, the closure temperature of He is usually less than 200 °C, whereas Ar is quantitatively retained in most minerals at 250 °C (Lippolt and Weigel, 1988; McDdougall and Harrison, 1988; Elliot et al., 1993). The MASW trapped in these samples preferentially acquired not only He, but also Ar from crustal rocks, implying that it was a relatively high-temperature fluid ($\geq$ 200 °C). This in turn requires an elevated geothermal gradient in this region before the MASW mixed with the mantle-derived fluid (see the discussion below).

4.2.2. Component 2: fluid from mantle-derived magma

Mantle-derived fluids are not only rich in ^{3}He but also poor in ^{36}Ar (Turner et al., 1993). Consequently, the only plausible source of the end-member rich in ^{3}He and poor in ^{36}Ar, as reflected by Figs. 2–4, is derived from the mantle. Extrapolating the trend in Fig. 5 to a likely mantle ^{3}He/^{4}He ratio of 6 Ra or so (the ^{3}He/^{4}He value of subcontinental mantle: Dunai and Baur, 1995; Gautheron and Moreira, 2002) implies a ^{40}Ar*/^{4}He of 0.3–0.7. This value is generally consistent with ^{40}Ar*/^{4}He of the subcontinent mantle (0.33–0.56: Burnard et al., 1998). Transport of fluids from the magma into the hydrothermal system did not significantly fractionate He from Ar. This is somewhat surprising as volatiles

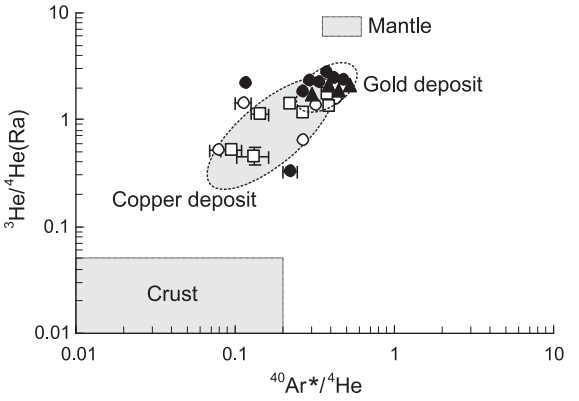

Fig. 5. ^{40}Ar*/^{4}He vs. ^{3}He/^{4}He (Ra) plot of inclusion trapped fluids in pyrite. Symbols and the Machangqing data source are the same as in Fig. 2.

produced by degassing of magmas is predicted to produce high $^{40}Ar^*/^4He$ ratios (e.g. Graham, 2002) due to the low solubility of Ar relative to He in silicate liquids. The lack of He–Ar fractionation implies efficient transfer of magmatic volatiles into the hydrothermal system.

The transport of mantle volatiles through the crust is closely linked to tectonic setting; mantle ^3He in crustal fluids is typically found in regions of crustal extension, thought to be released during intrusion of subsurface mantle-derived melts associated with extension (Oxburgh et al., 1986; Ballentine and Burnard, 2002). As described above, the deposits studied in this work are all located at both the exo- and endo-contact zones of alkali-porphyry rocks intruded in a crustal extension tectonic setting. Moreover, most ore minerals are disseminated in the mantle-derived alkaline porphyries (Table 1), suggesting almost no time gap between formation of the alkaline porphyries and mineralization. Therefore, the mantle-derived fluid end-member in the ore-forming fluids of the Red River–Jinshajiang ore deposits was most probably related to the mantle-derived alkaline magmatism, thus most likely representing a high temperature magmatic fluid.

4.3. Possible differences between gold and copper ore fluids

Assuming that the $^{36}Ar/^3He$ ratio of the fluid from mantle-derived alkaline magma was similar to that of the mantle ($\approx$ 1: Burnard et al., 1999; Moreira et al., 1998), it is possible to estimate the mantle compositions in a $^4He/^3He$ versus $^{36}Ar/^3He$ plot (Fig. 3). Least squares fitting suggests that the $^4He/^3He$ ratio of the magmatic fluid was $\sim$ 30,7000, equivalent to the $^3He/^4He$ ratio of $\sim$ 2.3 Ra and consistent with the $^3He/^4He$ trend shown in Fig. 4, but lower than that of potential subcontinental mantle He ($^3He/^4He \approx$ 6 Ra: Dunai and Baur, 1995; Gautheron and Moreira, 2002). Therefore, the magmatic fluids or their parent magma are themselves a mixture of radiogenic and mantle-derived noble gases. Within the magma, radiogenic He can be introduced during magmatic assimilation of crustal materials, or by "magma aging" where radiogenic He is produced in a long-lived magma chamber by decay of U-series elements within the molten magma. Both mechanisms have been invoked to explain unusually low He isotope ratios (less than MORB), such as those observed in hydrothermal ore deposits in Peru (Simmons et al., 1987), South Korea (Stuart et al., 1994) and China (Burnard et al., 1999). In the Red River–Jinshajiang region of Southwestern China, it has already been documented that the copper and gold ore hosted alkaline intrusions are the products of mantle-derived magma in which some crustal materials have been assimilated (Zhang et al., 1987; Chung et al., 1998; Hou et al., 2003; Bi et al., in press(b)). Consequently, the magmatic assimilation of crustal material could have been the main mechanism for diluting mantle He within the magma in the investigated intrusions.

However, when the gold and copper deposits are considered separately, the case is more complex. As suggested by Figs. 2–5, although the He and Ar isotope compositions of the gold and copper deposits follow the same trends, the ranges for gold deposits are different from the copper deposits. Generally, the fluids for the gold deposits are richer in ^3He and poorer in ^{36}Ar than those of the copper deposits, i.e. the gold deposits have higher $^3He/^4He$, $^{40}Ar/^{36}Ar$ and $^3He/^{36}Ar$ ratios than the copper deposits. The Machangqing copper deposit, geographically much closer to the Yao'an and Beiya gold deposits than to the Yulong copper deposit (Fig. 1), shares He and Ar isotopic features of the distant Yulong deposit instead of Yao'an and Beiya. Hence, this relationship appears to be related to the different ore types rather than being a local geographic phenomenon.

This difference indicates that the gold deposits have less MASW fluid than the copper deposits. The plot of $^4He/^3He$ vs. $^{36}Ar/^3He$ (Fig. 3) shows this very clearly; the higher the $^{36}Ar/^3He$ ratio, the higher the proportion of MASW. The amount of crustal assimilation by the parent magmas cannot affect this conclusion because neither ^3He nor ^{36}Ar will be assimilated. It is possible that crustal ^{36}Ar could have been assimilated by the magma, but this would require extensive crustal assimilation producing low $^3He/^4He$ ratios in contrast to the relatively high $^3He/^4He$ observed. The higher proportion of magmatic fluid during gold deposition is unexpected given that gold mineralization commonly forms at lower temperatures than copper deposits.

5. Conclusions

(1) Genetic links between the alkaline intrusion-hosted gold and copper mineralization and the mantle-derived alkaline magmatism exist in the Red River–Jinshajiang region. The ore-forming fluids of both the gold and copper deposits were differentiated from the mantle-derived alkaline magmas, but were further diluted by modified air-saturated water.
(2) The modified air-saturated water experienced an intensive interaction with crustal rocks before mixing with the magmatic fluids, inheriting crustal He and near-atmospheric Ar isotopic characteristics.
(3) Some differences between gold and copper deposits exist. The magmatic fluids responsible for the gold deposits were less extensively diluted by modified air-saturated water, resulting in higher $^{3}He/^{4}He$, $^{40}Ar/^{36}Ar$ and $^{3}He/^{36}Ar$ ratios than the copper deposits.

Acknowledgements

The authors are indebted to Prof. Ken Farley (California Institute of Technology) for making noble gas analytical facilities available to Ruizhong Hu. This research was supported jointly by an Outstanding Young Researcher Award from the National Natural Science Foundation of China (49925309), and grants from the Knowledge-innovation Program of the Chinese Academy of Sciences (KZCX3-SW-125, KZCX2-101) and the China National "973" Program (G1999043200). The manuscript benefitted from thoughtful reviews by M.A. Kendrick and D. Müller, for which the authors are extremely grateful. **[RR]**

References

Ballentine, C.J., Burnard, P.G., 2002. Production, release and transport of noble gases in the continental crust. Rev. Mineral. Geochem. 47, 481–538.

Bi, X.W., Cornell, D.H., Hu, R.Z., 2002. The origin of altered fluid: REE evidence from primary and secondary feldspars in the mineralization-alteration zone. Ore Geol. Rev. 19, 69–78.

Bi, X.W., Hu, R.Z., Cornell, D.H. The alkaline porphyry associated Yao'an gold deposit, Yunnan, China: rare earth element and stable isotope evidence for magmatic-hydrothermal ore formation. Miner. Depos. (in press(a)).

Bi, X.W., Hu, R.Z., Peng, J.T., Wu, K.X., Su, W.C., Zhan, X.Z. Geochemical characteristics of Yao'an and Machangqing alkaline intrusions. Acta Pet. Sin. (in Chinese with English abstract, in press(b)).

Burnard, P.G., Stuart, F., Ayliffe, L., Turner, G., Anonymous, 1993. Noble gas isotopic and elemental abundances in inclusion and vesicle trapped fluids: method. Seventh Meeting of the European Union of Geosciences; Abstract Supplement. Seventh Meeting of the European Union of Geosciences, vol. 5, Suppl. 1, p. 368.

Burnard, P.G., Farley, K.A., Turner, G., 1998. Multiple fluid pulses in a Samoan harzburgite. Chem. Geol. 147, 99–114.

Burnard, P.G., Hu, R.Z., Turner, G., Bi, X.W., 1999. Mantle, crustal and atmospheric noble gases in Ailaoshan gold deposits, Yunnan province, China. Geochim. Cosmochim. Acta 63, 1595–1604.

Burnard, P.G., Farley, K.A., 2000. Calibration of pressure-dependent sensitivity and discrimination in Nier-type noble gas ion sources. Geochem. Geophys. Geosystems 1 (paper number 2000GC00003).

Chung, S.L., Lee, T.Y., Lo, C.H., Wang, P.L., Cheng, C.Y., Yem, N.T., Hoa, T.T., Wu, G.Y., 1997. Intraplate extension prior to continental extrusion along the Ailao Shan-Red River shear zone. Geology 25, 311–314.

Chung, S.L., Lo, C.H., Lee, T.Y., Zhang, Y.Q., Xie, Y.W., Li, X.H., Wang, L.W., Wang, P.L., 1998. Diachronous uplift of the Tibetan plateau starting 40 Myr ago. Nature 394, 769–773.

Deng, W.M., Huang, X., Zhong, D.L., 1998. Petrological characteristics and genesis of Cenozoic alkali-rich porphyry in west Yunnan, China. Sci. Geol. Sin. 33, 412–425 (in Chinese with English abstract).

Dunai, T.J., Baur, H., 1995. Helium, neon and argon systematics of the European subcontinental mantle: implications for its geochemical evolution. Geochim. Cosmochim. Acta 59, 2767–2784.

Elliot, T., Ballentine, C.J., O'Nions, R.K., Ricchiuto, T., 1993. Carbon, helium, neon and argon isotopes in a Po basin natural gas field. Chem. Geol. 106, 429–440.

Gautheron, C., Moreira, M., 2002. Helium signature of the subcontinental lithospheric mantle. Earth Planet. Sci. Lett. 199, 39–47.

Graham, D.W., 2002. Noble gas isotope geochemistry of mid-ocean ridge and ocean island basalts: characterization of mantle source reservoirs. Rev. Mineral. Geochem. 47, 247–317.

Hou, Z.Q., Ma, H.W., Khin, Z., Zhang, Y.Q., Wang, M.J., Wang, Z., Pan, G.T., Tang, R.L., 2003. The Himalaya Yulong porphyry copper belt: product of large-scale strike-slip faulting in eastern Tibet. Econ. Geol. 98, 125–145.

Hu, R.Z., Burnard, P.G., Turner, G., Bi, X.W., 1998. Helium and argon systematics in fluid inclusions of Machangqing copper deposit in west Yunnan province, China. Chem. Geol. 146, 55–63.

Hu, R.Z., Bi, X.W., Burnard, P.G., Zhou, M.F., Zhao, J.H., Peng, J.T., Su, W.C., 2003. Mantle-derived gaseous components in the Xiangshan uranium deposit, Jiangxi Province, Southeastern China: He, Ar and C isotope evidences (submitted to Geochim. Cosmochim. Acta).

Jean-Baptiste, P., Fouquet, Y., 1996. Abandance and isotopic composition of helium in hydrothermal sulfides from the East Pacific Rise at 13N. Geochim. Cosmochim. Acta 60, 87–93.

Jensen, E.P., Barton, M.D., 2000. Gold deposits related to alkaline magmatism. In: Hagemann, S.G., Brown, P.E. (Eds.), Gold in 2000. Rev. Econ. Geol. vol. 13, pp. 279–314.

Kelley, K.D., Ludington, S., 2002. Cripple Creek and other alkaline-related gold deposits in the southern Rocky Mountains, USA: inference of regional tectonics. Miner. Depos. 37, 38–60.

Kendrick, M.A., Burgess, R., Pattrick, R.A.D., Turner, G., 2001. Fluid inclusion noble gas and halogen evidence on the origin of Cu-porphyry mineralizing fluids. Geochim. Cosmochim. Acta 65, 2651–2668.

Liang, Y.N., 1992. Geological features and ore-forming conditions of the Beiya porphyry gold deposit, Dali. J. Kunming Univ. Tech. 18 (3), 21–29 (in Chinese).

Lippolt, H.J., Weigel, E., 1988. ^{4}He diffusion in Ar-retentive minerals. Geochim. Cosmochim. Acta 52, 1449–1458.

Lottermoser, B.G., 1990. Rare earth element and heavy-metal behaviour associated with the epithermal gold deposit on Lihir Island, Papua New Guinea. J. Volcanol. Geotherm. Res. 40, 269–289.

Mamyrin, B.A., Tolstikhin, I., 1984. Helium Isotopes in Nature Elsevier, Amsterdam. 267 pp.

Marty, B., Jambon, A., Sano, Y., 1989. Helium isotope and CO_2 in volcanic gases of Japan. Chem. Geol. 76, 25–40.

Maughan, D.T., Keith, J.D., Christiansen, E.H., Pulsipher, T., Hattori, K., Evans, N.J., 2002. Contributions from mafic alkaline magmas to the Bingham porphyry Cu–Au–Mo deposit, Utah, USA. Miner. Depos. 37, 14–37.

McDdougall, I., Harrison, T.M., 1988. Geochronology and Thermochronology by the ^{40}Ar–^{39}Ar Method. Oxford Univ. Press, Oxford. 212 pp.

Moreira, M., Kunz, J., Allègre, C., 1998. Rare gas systematics in popping rock: isotopic and elemental compositions in the upper mantle. Science 279, 1178–1181.

Müller, D., 2002. Gold–copper mineralization in alkaline rocks. Miner. Depos. 37, 1–3.

Müller, D., Groves, D.I., 1993. Direct and indirect associations between potassic igneous rocks, shoshonites, and gold–copper deposits. Ore Geol. Rev. 8, 383–406.

Müller, D., Groves, D.I., 2000. Potassoic Igneous Rocks and Associated Gold–Copper Mineralization. Springer, Berlin. 252 pp.

Müller, D., Kaminski, K., Uhlig, S., Graupner, T., Herzig, P.H., Hunt, S., 2002. The transition from porphyry- to epithermal-style gold mineralization at Ladolam, Lihir Island, Papua New Guinea: a reconnaissance study. Miner. Depos. 37, 61–74.

Oxburgh, E.R., O'Nions, R.K., Hill, R.I., 1986. Helium isotopes in sedimentary basins. Nature 324, 632–635.

Qiu, H.N., 1996. ^{40}Ar/^{39}Ar dating of the quartz samples from two mineral deposits in western Yunnan (SW China) by crushing in vacuum. Chem. Geol. 127, 211–222.

Richards, J.P., 1992. Magmatic-epithermal transitions in alkalic systems: Porgera gold deposit, Papua New Guinea. Geology 20, 547–550.

Richards, J.P., 1993. The Porgera gold mine, Papua New Guinea: magmatic hydrothermal to epithermal evolution of an alkalic-type precious metal deposit. Econ. Geol. 88, 1017–1052.

Richards, J.P., McCulloch, M.T., Chappell, B.W., Kerrich, R., 1991. Sources of metals in the Porgera gold deposit, Papua New Guinea: evidence from alteration, isotope, and noble metal geochemistry. Geochim. Cosmochim. Acta 55, 565–580.

Rui, Z.R., Huang, C.K., 1984. Porphyry Copper (Molybdenum) Deposits in China Geological Publishing House, Beijing. In Chinese, 350 pp.

Sillitoe, R.H., 1997. Characteristics and controls of the largest porphyry copper–gold and epithermal gold deposits in the circum-Pacific region. Aust. J. Earth Sci. 44, 373–388.

Sillitoe, R.H., 2002. Some metallogenic features of gold and copper deposits related to alkaline rocks and consequences for exploration. Miner. Depos. 37, 4–13.

Simmons, S.F., Sawkins, F.J., Schlutter, D.J., 1987. Mantle-derived helium in two Peruvian hydrothermal ore deposits. Nature 329, 429–432.

Smith, P.E., Evensen, N.M., York, D., Szatmari, P., Oliveira, D.C., 2001. Single-crystal (super 40) Ar–(super 39) Ar dating of pyrite: no fool's clock. Geology 29, 403–406.

Strashimirov, S., Petrunov, R., Kanazirski, M., 2002. Porphyry-copper mineralisation in the central Srednogorie zone, Bulgaria. Miner. Depos. 37, 587–598.

Stuart, F.M., Turner, G., Duckworth, R.C., Fallick, A.E., 1994. Helium isotopes as tracers of trapped hydrothermal fluids in ocean-floor sulfides. Geology 22, 823–826.

Stuart, F.M., Burnard, P.G., Taylor, R.P., Turner, G., 1995. Resolving mantle and crustal contributions to ancient hydrothermal fluids: He–Ar isotopes in fluid inclusions from Dae Hwa W–Mo mineralisation, South Korea. Geochim. Cosmochim. Acta 59, 4663–4673.

Tang, R.L., Lo, H.S., 1995. Geology of the Yulong Porphyry Copper (Molybdenum) ore Belt, Tibet, China. Geological Publishing House, Beijing. In Chinese, 320 pp.

Torgersen, T., Kennedy, B.M., Hiyagon, H., 1988. Argon accumulation and the crustal degassing flux of ^{40}Ar in the Great Artesian Basin, Australia. Earth Planet. Sci. Lett. 92, 43–59.

Tu, G.C., Zhang, Y.Q., Zhao, Z.H., 1984. A preliminary study on the two alkali-rich intrusive rock belts in South China. In: Xu, K.Q., Tu, G.C. (Eds.), Geology of Granites and its Relations with Mineralization. Jiangsu Science and Technology Press, Nanjing, pp. 21–37. In Chinese.

Turner, G., Bannon, M.P., 1991. Argon isotope geochemistry of inclusion fluids from granite-associated mineral veins in southwest and northeast England. Geochim. Cosmochim. Acta 56, 227–243.

Turner, G., Stuart, F.M., 1992. Helium/heat ratios and deposition temperatures of sulphides from the ocean floor. Nature 357, 581–583.

Turner, G., Wang, S.S., 1992. Excess argon, crustal fluid and apparent isochrons from crushing K feldspar. Earth Planet. Sci. Lett. 110, 193–211.

Turner, G., Burnard, P.B., Ford, J.L., Gilmour, J.D., Lyon, I.C., Stuart, F.M., 1993. Tracing fluid sources and interaction. Philos. Trans. R. Soc. Lond., A 344, 127–140.

Turner, S., Arnaud, N., Liu, J., Rogers, N., Hawkesworth, C., Har-

ris, N., Kelley, S., VanCalsteren, P., Deng, W., 1996. Post-collision, shoshonitic volcanism on the Tibetan plateau: implications for convective thinning of the lithosphere and the source of ocean island basalts. J. Petrol. 37, 45–71.

Wang, J.H., Yin, A., Harrison, T.M., Grove, M., Zhang, Y.Q., Xie, Y.W., 2001. A tectonic model for Cenozoic igneous activities in the eastern Indo–Asian collision zone. Earth Planet. Sci. Lett. 188, 123–133.

Ye, T.Q., Hu, Y.Z., Yang, Y.Q., 1992. Geochemical Background and Mineralization of Au, Ag, Pb and Zn in San Jiang Region Geological Publishing House, Beijing (in Chinese), 256 pp.

Yin, A., Harrison, T.M., 2000. Geologic evolution of the Himalayan–Tibetan orogen. Annu. Rev. Earth Planet. Sci. 28, 211–280.

York, D., Masliwec, A., Kuybida, P., Hanes, J.E., Hall, C.M., Kenyon, W.J., Spooner, E.T.C., Scott, S.D., 1982. (super 40) Ar/(super 39) Ar dating of pyrite. Nature 300, 52–53.

Zhang, Y.Q., Xie, Y.W., 1997. Chronology and Nd–Sr isotopes of the Ailaoshan-Jinshajiang alkali-rich intrusions. Sci. China 27, 289–293 (in Chinese).

Zhang, Y.Q., Xie, Y.W., Tu, G.C., 1987. A preliminary study on the relationship between rift and Ailaoshan-Jianshajiang alkaline intrusive rocks. Acta Pet. Sin. 3, 17–25 (in Chinese with English abstract).

Zhang, Y.Q., Xie, Y.W., Qiu, H.N., Li, X.H., Zhong, S.L., 1998. Petrogenesis series and the ore-bearing porphyrites of the Yulong copper ore belt in eastern Tibet. Geochimica 27, 236–243 (in Chinese with English abstract).